

Bulklike band-offset mystery solved through energy minimization: Lessons from perovskite oxide heterojunctions

Raymond T. Tung^{1,*} and Leeor Kronik^{2,†}

¹*Department of Physics, Brooklyn College, CUNY, Brooklyn, New York 11210, USA
and Graduate Center, CUNY, New York, New York 10016, USA*

²*Department of Materials and Interfaces, Weizmann Institute of Science, Rehovoth 76100, Israel*



(Received 18 September 2018; revised manuscript received 8 January 2019; published 4 March 2019)

The formation of band offset (BO) at isovalent semiconductor heterojunctions has been branded “bulklike” because of an insensitivity of the BO to the interface orientation and atomic structure and a transitivity in BOs. Even though tunability and nontransitivity of BO are frequently found for heterovalent interfaces, empirical theories with built-in bulklike characteristics have thus far dominated the explanation of experimental BOs. Presently, the distribution of charge density and the formation of BO at a large number of interfaces between lattice-matched perovskite oxides are studied in detail using density functional theory. Ionic screening is found to dominate the formation of the BO, as a sharp dependence of the (apparently tunable) BO on atomic structure for unrelaxed interfaces is essentially washed out upon lattice relaxation. Numerical experimentation with deliberate embedding of dipolar layers in perovskite oxides and their interfaces corroborates the effectiveness of ionic screening. The relaxed, converged (bulklike) BOs are found to be in good agreement with the prediction of the neutral polyhedra theory (NPT). The success of the NPT, presently for ionic interfaces and previously for covalent zinc-blende interfaces, unmasks a possible connection between the partition into neutral symmetric cells and the energy-minimization requirement on the interface charge distribution. The independence of the BO on interface specifics, i.e., bulklike behavior, is shown to stem directly from such a property of charge distribution with minimized electrostatic energy. As energy minimization governs the formation of charge distribution in general, NPT is expected to describe the band offset of a wide variety of material interfaces.

DOI: [10.1103/PhysRevB.99.115302](https://doi.org/10.1103/PhysRevB.99.115302)

I. INTRODUCTION

The band offset (BO) for isovalent semiconductor heterojunctions is often found to be independent of interface orientation, atomic structure, and abruptness [1], and follows a transitivity rule [2–4]. This has led to the suggestion that the BO depends only on bulk properties of the constituents [1], i.e., the formation mechanism is “bulklike.” Many models with a built-in bulklike mechanism were proposed to explain experimentally observed BOs [1,5]. The most common of these suggested the alignment of a specific feature in the band structure of the semiconductor, such as the charge neutrality level [6–8] or impurity/defect levels [9,10]. Quite the opposite behavior, namely, significant tunability and nontransitivity of the BO, has been found experimentally for heterovalent interfaces [11–14]. Because the magnitude of the BO is a direct result of the equilibrium charge distribution at the heterojunction interface, and the formation of the latter is governed by energy minimization, the observed bulklike behavior for some interfaces and tunability for others must both have explanations within the concept of energy minimization. In the present work, charge distribution at heterojunctions between lattice-matched perovskite oxides is investigated in detail to shed light on these issues.

Perovskite oxides have attracted much attention because of a richness in their dielectric, ferroelectric [15,16], piezoelectric [17], ferromagnetic, resistance switching [18], and other properties that are suitable for applications. In particular, the discovery of a two-dimensional electron gas (2DEG) at polar heterojunction interfaces between perovskite oxides led to much basic and application-oriented scientific interest [19–22]. The BO between an oxide and a semiconductor or between two oxides is an important interface property [1,23] that has been investigated both experimentally and theoretically [4,24–26]. Experimental BO results have been closely reproduced from first principles using density functional theory (DFT) based on hybrid-functional calculations, with the exact-exchange fraction optimized individually for bulk perovskite oxides [27]. Such calculations have emerged as a convenient and reliable method for both oxide and semiconductor interfaces [21,27–31].

While great strides have been made in the computation of the experimentally observed BOs at oxide interfaces, the physical picture of the mechanisms of BO formation has remained largely at the stage of empirical models [1]. As discussed previously [32,33], the valence-band offset (VBO) at a heterojunction between two semiconductors or insulators A and B , Φ_{VBO}^{A-B} , can be decomposed into two bulk terms and one interface term:

$$\Phi_{\text{VBO}}^{A-B} = \mu_A - \mu_B + e\Delta_{\text{int}}. \quad (1)$$

*rtung@brooklyn.cuny.edu

†leeor.kronik@weizmann.ac.il

In the above equation μ , the internal chemical potential, is the difference between the valence-band maximum (VBM) and the average electrostatic potential energy on either side of the junction. The interface dipolar term, $e\Delta_{\text{int}}$, is the difference between the averaged electrostatic potential energies across the interface. Being a purely intensive property, μ is obtainable from a bulk calculation with periodic boundary conditions. The only term in Eq. (1) that is not known *a priori* for any heterojunction is $e\Delta_{\text{int}}$, which is purely electrostatic in nature, as it results entirely from the charge distribution in the interface region. Therefore, a comprehensive explanation of the magnitude of BO can be obtained if one is able to predict the equilibrium charge distribution at heterojunction interfaces. Recently, we have shown that this can indeed be achieved for interfaces between covalent semiconductors with zinc-blende/diamond structures [34,35]. Specifically, we showed that thanks to the nearsightedness of many-electrons systems [36], the equilibrium charge density at those interfaces is well predicted by model solids constructed of neutral polyhedra obtained from a knowledge of the charge distribution in bulk semiconductors [34]. The success of neutral polyhedra theory (NPT) in reproducing first-principles computational data appears to be rooted in the ease with which the charge distribution associated with the strongly directional bonding in zinc-blende/diamond covalent semiconductors can be precisely predicted. NPT would then seem applicable only to such covalent systems. In the present work, charge distribution at perovskite oxide interfaces is analyzed in detail in search of a density-based approach, perhaps different from NPT, that is suitable for modeling the BO at ionically bonded interfaces.

II. COMPUTATIONAL APPROACH

All perovskite oxides studied in this work were calculated in the cubic structure, with some oxides that ordinarily occupy the orthorhombic crystal structure studied with lattice parameters optimized in cubic lattice. The perovskite oxides studied belong to three groups—“II-IV-Ox”, “I-V-Ox”, and “III-III-Ox”—based on the formal charge states of the cations occupying the corner sites and the body-center sites, with the oxygen atoms occupying the face-center positions. All calculations were spin unpolarized, such that magnetic properties, exhibited by some oxides, were suppressed. To simulate heterojunctions between oxides, supercells containing back-to-back heterointerfaces in the (100), (110), or (111) orientations were investigated for BO determination, while making sure that the supercell is large enough to avoid spurious effects of the periodicity on the interface behavior. Lattice-matching considerations have led to the study of both isovalent interfaces (e.g., between CaHfO_3 and SrSnO_3 , both of the II-IV-Ox group) and heterovalent interfaces (e.g., between one II-IV-Ox oxide and an oxide from either the I-V-Ox, e.g., KTaO_3 , or the III-III-Ox, e.g., LaGaO_3 , groups).

Heterojunctions between isovalent, lattice-matched, perovskite oxides can be constructed with any orientation. For planar interfaces with polar orientations, such as (100) and (111), there are two possible atomic arrangements between oxides without common cations. For example, between CaHfO_3 and SrSnO_3 , there could be an interface with corner

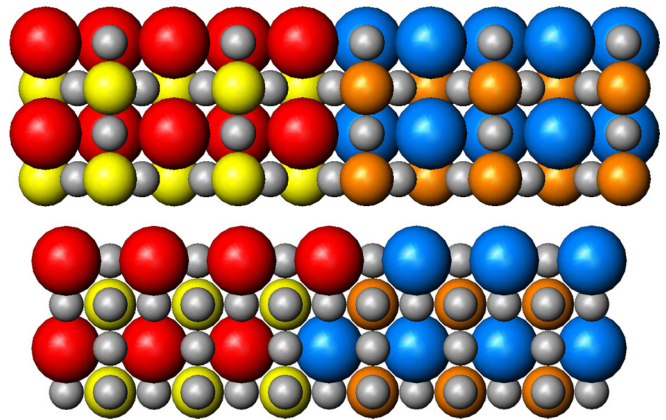


FIG. 1. Ball-and-stick models for interfaces between perovskite oxides: (top) planar (110) and (bottom) (100) interface with mixed-corner cations. Large spheres represent corner-cation atoms, medium-sized spheres represent body-center metal atoms, and small light-colored spheres represent oxygen atoms. Color is used to distinguish chemical species. The interface plane for (bottom) contains oxygen atoms and a 50-50 mixture of the two corner-cation kinds.

cations (CC) of the first oxide, Ca, and body-centered (BC) metal atoms of the second oxide, Sn, on adjacent planes, along with stoichiometric oxygen atoms. Such an interface is distinctive from one with BC Hf atoms and CC Sr atoms occupying adjacent planes. These two types of interfaces are referred to below as CC1-BC2 and BC1-CC2 interfaces, respectively.

While isovalent oxide interfaces can be constructed in any orientation without interface charging (as is the case in compound semiconductor interfaces [35]), planar heterovalent oxide interfaces are “charged” along polar directions. (The most famous examples are charged interfaces that exhibit 2DEG [19], although the much-lower-than-expected 2DEG densities observed experimentally would suggest that these interfaces exhibit a mixed structure [37–39].) In the present work, which is focused on BO formation mechanism(s), only interfaces that are neutral and therefore free from free carrier complications were studied in detail. As shown in Table SM1 of the Supplemental Material (SM) [40] for two instructive test cases, the non-neutral interfaces are not favored energetically. A ball-and-stick model of a nonpolar planar (110) interface is shown in Fig. 1. Along the polar (100) or (111) direction, analyses similar to those previously used in the design of neutral heterovalent interfaces between compound semiconductors [35] suggest that a 1:1 mixture of the two corner cations on a common interface plane separating the two perovskite oxide crystals should lead to interface neutrality. A (100) heterojunction with mixed corner atoms is shown in Fig. 1, with some models of other interface orientations and atomic arrangements given in Fig. SM1 of the SM [40]. For example, a (100) interface between the II-IV-Ox BaTiO_3 and the I-V-Ox KTaO_3 has a stacking sequence of $-\text{BaO}-\text{TiO}_2-(\text{Ba}_{0.5}\text{K}_{0.5})\text{O}-\text{TaO}_2-\text{KO}-$ at the “mixed BaK” interface. A similar analysis also suggests that a 1:1 mixed plane of the BC species should result in neutral interfaces. The plane-by-plane sequence at such a mixed-TiTa (111) interface between the same two oxides would be $-\text{Ti}-\text{BaO}_3-\text{Ti}_{0.5}\text{Ta}_{0.5}-\text{KO}_3-\text{Ta}-$

Mixed atomic species on the interface plane are simulated by doubling the two-dimensional unit cell in size to accommodate each of the two distinct atoms.

All DFT calculations presented in this work were performed using a plane-wave basis, along with a projector augmented wave treatment of core electrons, as implemented in the Vienna Ab initio Simulation Package (VASP) [41–43]. Bulk calculations were performed using the generalized-gradient approximation (GGA) functional of Perdew, Burke, and Ernzerhof (PBE) [44], as well as the conventional hybrid functional (PBE0) [45] and the screened hybrid functional (Heyd-Scuseria-Ernzerhof, HSE) [46,47] that are based on PBE. Each supercell was initially calculated in the unrelaxed structure, i.e., with all atoms clamped to their bulk positions. At least four layers of atoms at each interface were then allowed to relax, using the PBE functional for energy minimization. The smaller (~ 60 atoms) of all fully relaxed supercells were also studied with the HSE functional, with some supercells further studied with the PBE0 functional for comparison.

Valence-band offsets (VBOs) were deduced using Eq. (1) [34,35]. The interface dipolar term in this equation was computed from differences in the average potential energy across an interface. The chemical potential terms in the equation were obtained by mapping the valence-band maximum (VBM) position with respect to the average potential energy, using a calculation of the bulk oxide residing on either side of the heterojunction interface. Throughout, and in agreement with previous work [28,48], differences in the average potential energy across an interface were found not to be significantly affected by the type of functional used for the calculation, with a difference smaller than 0.15 eV. Two examples are shown in Fig. SM2 of the SM [40] to illustrate this insensitivity of junction charge distribution to functionals, with the similarity between HSE and PBE0 results for the VBO demonstrated in Table SM2 of the SM [40]. Furthermore, as previously pointed out [49], none of the heterojunctions studied in this work suffers from qualitative errors in the charge density due to band-gap errors. Therefore, for BO determination, it suffices to rely on charge densities calculated for large supercells with the PBE functional. Because band-edge positions for bulk oxides and semiconductors may vary significantly with the functional used in the calculation, we used HSE-based values. We note, however, that the comparison of DFT-calculated VBOs with values obtained from model solids, discussed in detail below, relies only on the electrostatics across the interface and is therefore essentially independent of the functional used for VBM determination.

Model solids for the bulk oxides were constructed based on Bader’s atoms in molecule (AIM) analysis, which renders basins associated with individual ions [50–53]. A corner-cation-centered (CCC) Bader model solid of the perovskite oxide was constructed from a building block that anchors on one corner-cation Bader atom, surrounded by 1/8 of the transition-metal Bader atoms at the eight body-center positions, and 1/4 oxygen Bader atoms at the 12 face-centered positions. Alternatively, a building block centered on one full transition-metal Bader atom at the body-centered position, 1/8 of the Bader corner cations at the eight corner positions,

and 1/2 oxygen Bader atoms at the six face-centered positions can be used to construct a body-center-atom-centered (BAC) Bader model solid. Building blocks centered on oxygen Bader atom can also be used to construct model solids, but offered no additional advantage in analysis and were not employed. For either model solid, the building block is itself devoid of net monopole, dipole, or quadrupole moments, resulting in the absence of long-range external electric fields. The calculation of the potential energy for a model solid based on Bader atoms, averaged over each unit cell, has been discussed previously [33] and is explained in detail in Discussion SM1 of the SM [40] for the perovskite structure. Charge densities calculated for supercells were also analyzed by the Bader method, for comparison with bulk results.

The charge distribution in the bulk crystal has also been analyzed using NPT, which proposes the partition of the density into neutral regions and the construction of a model solid by stacking these neutral regions together. For covalent semiconductors, it appeared natural to employ a planar boundary to partition each directional bond into two neutral parts [34]. The model-solid potential was then simply related to the sum of the spherapoles of all neutral polyhedra in a unit cell [34], where the spherapole for a polyhedron is defined as [33]

$$\Theta_{\text{polyh}} = \int r^2 \rho(\vec{r}) d\vec{r} \quad (2)$$

with $\rho(\vec{r})$ being the charge density. For “ionic” perovskite oxides, the absence of directional bonds may seem to leave the strategy for neutral partitioning open. However, as explained in detailed in Discussion SM2 of the SM [40], a planar boundary perpendicular to a line connecting two atomic positions represents a stationary solution to a minimized sum of spherapoles, under the constraint that the charge within each region is conserved. Therefore, the use of planar facets partitions the charge distribution of a unit cell into neutral polyhedra with a total spherapole that is minimal, independent of the bonding type or the structure of the crystal. The average potential of the presently employed model solid based on neutral polyhedra is then minimal among all possible ways to construct model solids from atom-centered neutral cells [54]. This NPT potential energy thus reflects a fundamental property of a bulk charge distribution, corresponding to a maximally confined electric field. The main results of NPT analysis of bulk perovskite oxides can be found in Table II, with additional volume information described in Table SM3 of the Supplemental Material [40].

III. DFT RESULTS

DFT calculations of the VBO at unrelaxed isovalent perovskite interfaces, shown in Fig. 2 (on the left for each interface), indicate that the VBO is nearly independent of the interface atomic arrangement and orientation. Furthermore, the VBO does not change significantly (by at most 0.25 eV) when the interface structure is allowed to relax (on the right for each interface in Fig. 2). Due to differences in cation size, the two possible structures of a polar interface (CC1-BC2 and BC1-CC2) typically relax with small expansion/contraction of opposite signs. In agreement with previous reports [4,55], the absolute values of the VBOs found for the relaxed iso-

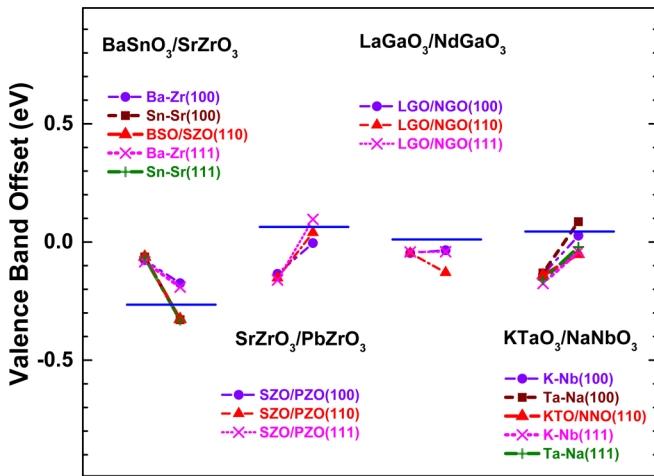


FIG. 2. Valence-band offsets calculated for isovalent heterojunctions of perovskite oxides. The orientation and the atomic arrangement of the interface are marked by the identities of atoms on interface planes, where distinction is necessary. For example, under the $\text{BaSnO}_3/\text{SrZrO}_3$ heading, the Ba-Zr(100) is a (100) interface with Ba and Zr on adjacent planes, and the BSO/SZO(110) is a planar (110) interface between these two oxides. Within each group, the data shown on the left are VBO's calculated for unrelaxed, clamped interfaces and those shown on the right are from the final, relaxed interfaces. The VBO predicted by the NPT with face density correction for each heterojunction is drawn as a horizontal solid bar.

valent heterojunctions are small, <0.4 eV, resulting in the conduction-band offset accounting for much of the difference between the two band gaps. Also indicated on Fig. 2 are the VBOs expected for each of the oxide heterojunctions from NPT.

Turning to heterovalent junctions, we first consider the macroscopically averaged electrostatic potential energy curves across the junction. An example, using the $\text{BaTiO}_3/\text{KTaO}_3$ junction, is shown in Fig. 3 for various interface orientations and compositions, both before and after relaxation. The fact that the average potential is nearly constant in the bulk oxide regions of all curves establishes that these interfaces are indeed neutral [35]. For the unrelaxed interface, the change in the average potential energy across the interface shows a large dependence, of as much as ~ 2 eV, on the atomic structure and orientation of the interface (see top part of Fig. 3). This shows that unlike in the unrelaxed isovalent case, there is significant variation of the VBO. However, when the heterovalent interfaces are allowed to relax, the charge distribution and associated potential energy profile are significantly modified. As shown in the lower part of Fig. 3, the shifts in the average potential energy across the interface, widely scattered for the unrelaxed interfaces, collapse into a narrow range upon relaxation. Figure 4 graphically captures these changes in the VBOs, with unrelaxed interfaces plotted on the left of each group and the relaxed VBOs on the right. Numerical values for the VBO of relaxed heterojunction are tabulated in Table III. Lattice relaxation renders the VBO for neutral heterovalent heterojunction between two perovskite oxides essentially independent of interface orientation and initial atomic arrangement, as shown in Fig. 4. The implica-

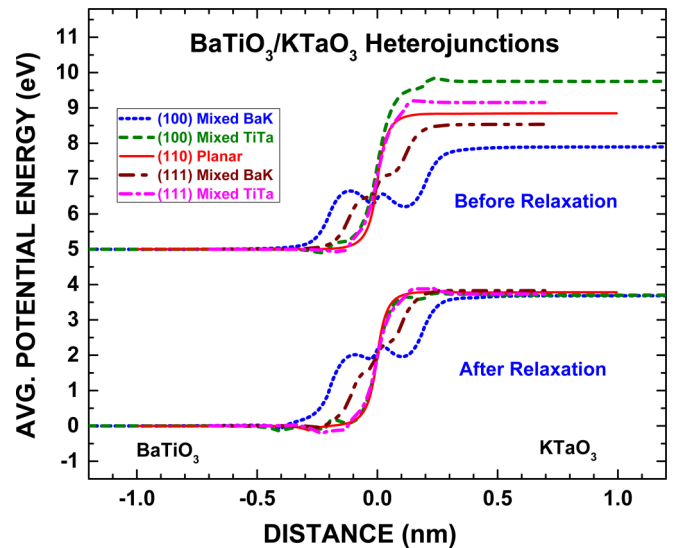


FIG. 3. Macroscopically averaged potential energy distributions calculated for neutral $\text{BaTiO}_3/\text{KTaO}_3$ interfaces. The orientation and the atomic arrangement of the interface are as marked. Curves are vertically shifted for clarity. For each interface, the potential distribution before and after lattice relaxation is shown in the upper and lower part of the figure. The significant dependence of the potential energy offset on interface orientation and atomic arrangement before relaxation becomes negligible after the lattice is relaxed.

tions of Figs. 2–4 are striking. Taken together, they show that independent of the interface orientation and atomic arrangement one starts out with, the relaxation process governs the formation of BO, as only then does the final VBO emerge. This relaxation process can be referred to as “ionic screening”: The shifts in ion positions, driven by nonzero electric fields, by and large screen out the difference in initial dipoles at the unrelaxed interfaces.

An additional perspective of the ionic screening effect is obtained by considering the embedding of a submonolayer of heterovalent polar pairs into perovskite oxides, i.e., the creation of an “artificial” dipolar interface in an otherwise bulk structure. The embedded heterovalent pairs are chosen to be nominally lattice matched to the hosts, to minimize effects due to strain. For example, one-half monolayer of II-IV SrTi pairs can be embedded in the III-III-Ox LaGaO_3 (because of the lattice-matching condition between LaGaO_3 and SrTiO_3) and complementarily, one-half monolayer of III-III LaGa pairs can be embedded into SrTiO_3 . A second example involves similar cross embedding of polar pairs between the lattice-matched II-IV-Ox BaTiO_3 and I-V-Ox KTaO_3 . Profiles of the macroscopically averaged electrostatic potential energy distributions obtained from such “embedded homojunctions” are given in Fig. 5. Clearly, the as-embedded heterovalent pairs induce large potential energy offsets (>1.5 eV) in the bulk oxide, with a sign consistent with the polarity of the embedded dipole. However, here too these large potential energy shifts are almost completely wiped out after lattice relaxation. This is markedly different from the results of similar calculations for covalent semiconductors, where large starting potential shifts due to embedded heterovalent pairs remained largely intact even after relaxation [35]. The consequences of

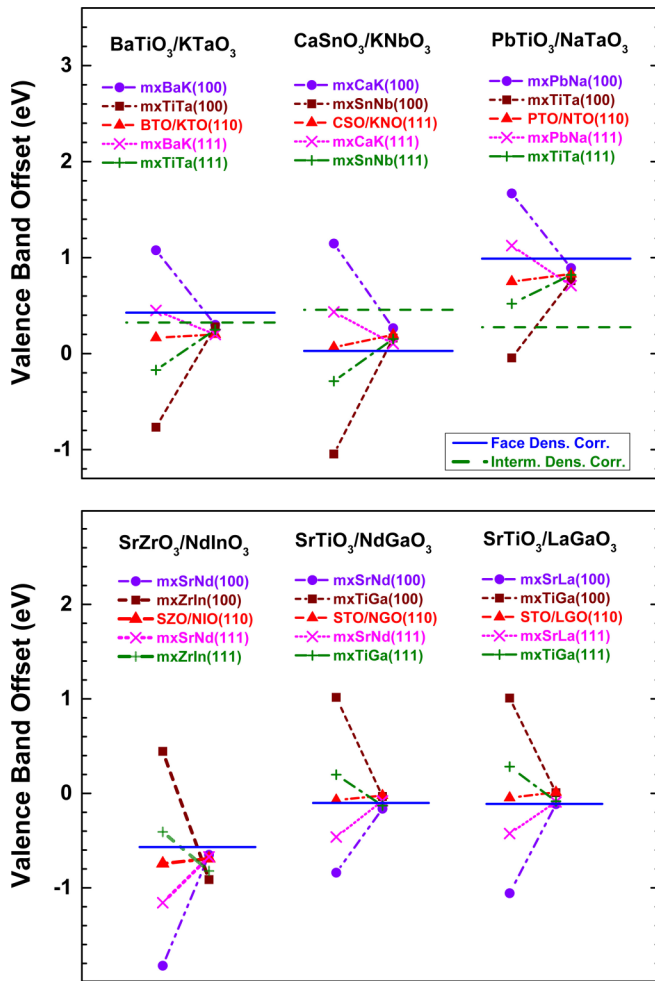


FIG. 4. Valence-band offsets calculated for heterovalent (top) II-IV-Ox/I-V-Ox and (bottom) II-IV-Ox/III-III-Ox heterojunctions of perovskite oxides. The orientation and the atomic arrangement of the interface are marked by atoms on the interface plane, when necessary. For example, from the $\text{BaTiO}_3/\text{KTaO}_3$ group, “mxBaK(100)” is a (100) interface with 50-50 mixture of Ba and K, and an appropriate number of oxygen atoms, on the interface plane. Within each group, the data shown on the left are VBO’s calculated for unrelaxed, clamped interfaces and those shown on the right are from the final, relaxed interfaces. The VBO predicted for each heterojunction by the NPT with corrections for density on the polyhedra face is drawn as a horizontal solid bar. In the top panel, the NPT predictions corrected according to the intermediate density are also shown, as broken horizontal bars.

similar embedding at several isovalent interfaces are given in Fig. 6. Once again, the inserted dipoles lead to large potential energy shifts, $>2\text{eV}$, for the unrelaxed interfaces (see inset of Fig. 6), but upon lattice relaxation the induced potential energy shifts become much smaller, often (but not always) to the point of being indistinguishable from those of the unembedded interfaces. Thus, the results of Figs. 5 and 6 show that unlike the tunability in BO demonstrated previously for heterovalent heterojunctions of covalent semiconductors [35], ionic screening makes it very difficult to adjust the VBO of a perovskite heterojunction by means of dipole alteration through interface modification.

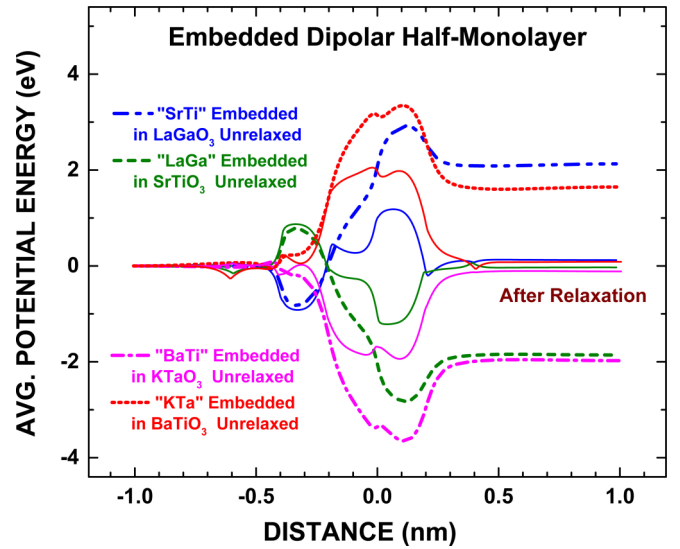


FIG. 5. Macroscopically averaged electrostatic potential energy distributions calculated for perovskite oxide embedded with one-half monolayer of heterovalent pairs in the $\langle 100 \rangle$ direction. Before relaxation, the results for SrTi embedded in LaGaO_3 , LaGa embedded in SrTiO_3 , BaTi embedded in KTaO_3 , and KTa embedded in BaTiO_3 are shown as dash-dot-dotted, dashed, dash-dotted, and dotted lines, respectively. Potential distributions after relaxation are shown as thin solid lines.

IV. BADER AND NPT ANALYSES

VBO systematics for the *unrelaxed* heterojunctions, shown in Figs. 3 and 4, can be understood with the help of Bader model solids. VBM positions, calculated for such solids based on results obtained with the HSE functional, are given in Table II, with corresponding volumes given in Table SM3 of the SM [40]. These results include a correction for the offset between the average electrostatic potential energy calculated for the model solid and the average potential energy computed by DFT, arising from the use of pseudopotentials in the latter. As previously shown [34], this correction is performed by equating the DFT and model-solid potential energy profiles in interstitial positions.

For unrelaxed II-IV-Ox/I-V-Ox interfaces, junctions with mixed corner cations and mixed body-center atoms invariably exhibit larger and smaller VBOs, respectively, compared to those found for the planar (110) interface. Bader analyses of these and other interfaces show that the charges for interface atoms are only slightly modified from their respective values in bulk oxides, which now provides a basis for explaining the observed systematics. If one assumes that the charge distribution of all Bader atoms at the interface is frozen at its bulk distribution, then the VBO of the five unrelaxed interfaces between heterovalent oxides [the mixed-BC (100), the mixed-CC (100), the planar (110), the mixed-BC (111), and the mixed-CC (111)] would simply be given by the differences between the VBM values of the two oxides in the five consecutive columns in Table II. Using the $\text{BaTiO}_3/\text{KTaO}_3$ heterojunction as an example, the VBOs deduced from this Bader model-solid analysis for the mixed-BaK(100), the mixed-TiTa(100), the (110), the mixed-BaK(111), and the

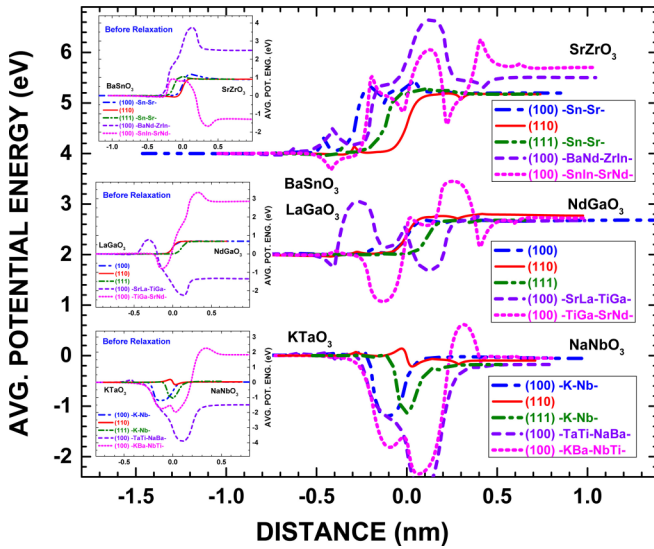


FIG. 6. Macroscopically averaged potential energy distributions calculated for isovalent $\text{BaSnO}_3/\text{SrZrO}_3$ (upper), $\text{LaGaO}_3/\text{NdGaO}_3$ (middle), and $\text{KTaO}_3/\text{NaNbO}_3$ (lower) interfaces. The orientation and the atomic arrangement of the interface are as marked. Included are results for (100) interfaces that have been embedded with one-half monolayer of heterovalent pairs. NdIn pairs are used for the upper II-IV-Ox heterojunction, SrTi pairs for the middle III-III-Ox heterojunction, and BaTi pairs for the lower I-V-Ox heterojunction. The embedded interfaces are marked by identities of atoms on consecutive interface planes. For example, the “(100)–SrLa–TiGa–” interface (upper) has a stack of $-\text{GaO}_2-(\text{Sr}_{0.5}\text{La}_{0.5})\text{O}-(\text{Ti}_{0.5}\text{Ga}_{0.5})\text{O}_2-\text{NdO}-$ planes separating pure LaGaO_3 and NdGaO_3 . The embedded dipoles lead to large potential energy shifts for the unrelaxed interfaces, as shown in the insets. After relaxation, these huge shifts all but disappear, as shown in the main panel.

mixed-TiTa(111) interfaces would be +4.17, -2.58 , +0.21, +1.52, and +0.07 eV, respectively. Supercell calculations yield values of +1.08, -0.77 , +0.16, +0.45, and -0.17 eV, respectively, for the same five interfaces, i.e., the trend predicted by the Bader analysis is correct, although the range of VBOs is less than predicted. The latter is likely due to the redistribution of charge within each Bader atom, arising from changes in the chemical environment, that occur even though the net Bader charge remains essentially unchanged from bulk value. Thus, the strong dependence of the VBO on the orientation and structure of the unrelaxed heterovalent interface is attributable to ionic charges being held at fixed positions at the interface.

Clearly, the most significant and surprising finding of the present work is the disappearance of the sharp dependence of the VBO on the atomic arrangement and orientation upon lattice relaxation. Seemingly responsible for the final BO, the lattice relaxation process needs to be carefully considered here in order to understand the VBO at relaxed perovskite oxide interfaces. With either an unrelaxed interface or a relaxed interface, the electronic optimization process in a DFT calculation is identical. The difference between the unrelaxed and relaxed calculations is that in the latter, the Hellmann-Feynman force [56] on each atom is required to be zero (in practice, smaller than some small numerical limit) through position optimiza-

tion, whereas the forces are not managed for the former. It thus appears likely that the nulling of electric field at all atomic sites has a dominant effect on the charge distribution and the BO at the relaxed interface. It seems plausible that the final BO could then be explained, or even derived, simply from this requirement for the electric field to vanish.

To explore the effect on charge distribution of the condition of vanishing electric field at all ion core sites, we first consider a “thought experiment” on one possible method to construct such a charge distribution. It is known that external to a “symmetric neutral cell” of charge distribution possessing no net charge, dipole moment, or quadrupole moments, the electric field falls off rapidly and may thus be ignored [33]. If such a neutral cell is to contain a single atom and to be centered about the atomic position, as in NPT, the internal electric field due to its own charge must vanish at the central atomic position, from symmetry. Therefore, when symmetric neutral cells, not all of which are necessarily identical, are used to build a volume of charge distribution, the electric field on any internal atomic site vanishes because neither the charge distribution within its own cell nor the charge distribution from any neighboring cell provides a nonzero contribution. Thus, any charge distribution put together by stacking symmetric neutral cells necessarily satisfies the zero-field condition required of relaxed structures. Such an assembled charge density, which induces no external electric field, would have no influence on the potential distribution outside of its confines. Therefore, if a certain volume is known to be stackable from symmetric neutral cells, then the charge inside this volume can be completely ignored as far as the potential distribution elsewhere is concerned. It follows that for the BO problem at hand, any region of the interface where the charge distribution is known to be decomposable into symmetric neutral cells is irrelevant for the purpose of BO computation, regardless of the precise position, chemical identity, or shape of the symmetric neutral cells.

While distributions constructed with symmetric neutral cells must have vanishing electric fields at its atomic sites, the reverse statement (i.e., that charge distributions with vanishing field at atomic sites are stackable from symmetric neutral cells) is not necessarily correct. NPT would only be suitable for the BO of perovskite oxides if there are reasons to expect that the interface charge distribution may be approximated by stacked symmetric neutral cells. One factor that would preclude such an expectation is significant charge transfer. Indeed, in our previous studies of zinc-blende heterojunctions, we found that NPT was quite successful with relaxed *isovalent* junctions [34] but not able to account, by itself, for the wide range of BOs calculated for relaxed *heterovalent* junctions [35]. From quadrant-by-quadrant analysis of zinc-blende interfaces, charge transfer was found to be significant ($>0.1e$) at heterovalent interfaces, but was largely absent for isovalent interfaces [35]. Subsequent Bader analysis shows that the charge for atoms at some zinc-blende interfaces is different by more than $0.2e$ ($>30\%$) from its value in the bulk [57]. In the presence of heterovalent covalent bonds, the interface charge density can still be partitioned into individual cells that are electrically neutral, but the charge distribution can no longer be symmetric within all cells. This will result in nonvanishing dipole moments for these cells, which would mean that their contribution toward the formation of the zinc-blende BO

cannot be ignored. At any of the neutral perovskite oxide interfaces studied in this work, Bader analysis shows that the net charge for cations rarely differs by more than $0.02e$ from its bulk value. Oxygen Bader charges on the interface plane of a heterovalent heterojunction may differ by as much as $0.06e$ from that of either of the two bulk oxides (see Table II). However, changes in oxygen charge are dictated by the overall neutrality of the interface and have little effect on the BO because the direction of such charge transfer is parallel to the interface. The significant shifts in BO associated with relaxation of perovskite oxide interfaces are thus mainly a result of ionic movement and not of charge transfer between ions, in agreement with what is generally expected of ionic compounds.

Without significant charge transfer, the charge distribution at perovskite oxide interface appears at least amenable to modeling with NPT. The actual applicability of NPT for perovskite oxide interfaces rests on the presence of symmetry in charge distribution around each ion/atom. To see that this is not an unreasonable assumption, one first uses the fact that the Bader charge of any atom remains approximately unchanged to reduce each Bader atom to a point charge of fixed quantity. The total energy of such a model system is the electrostatic potential energy, the minimization of which using the variational principle yields the equilibrium positions for all point charges. These are locations where the electric field vanishes and, because of the importance of potential energy for ionic systems, these are approximate locations where actual ions relax to. One now replaces each point charge with the (frozen) charge distribution of bulk Bader atoms.

Because of the internal symmetry of bulk Bader atoms, the electric field still vanishes on all atomic sites immediately after the switch. Furthermore, because of the absence of field on atomic sites initially, it is reasonable to expect the charge distributions about atomic sites to remain largely symmetric when the rigid Bader charge densities are allowed to relax. Thus, with its main underlying assumption on the symmetric of charge distribution about each atomic position appearing justifiable, NPT can be used to model the BOs of perovskite oxides. One notes that an important consequence/requirement of the NPT, namely, that the perovskite oxide BO is insensitive to interface orientation and atomic structure, is already borne out by supercell calculations.

VBM values for NPT model solids are given in Table III, with volume information given in Table SM3 of the SM [40]. To model the BO of perovskite oxides with NPT, one starts with the charge distribution of an entire heterojunction and partitions the two bulk oxide regions away from the interface into neutral polyhedra. This step is valid because neutral polyhedra are obtained from such partition in the first place. Between the two NPT model solids is the interface specific region (ISR), which borders on neutral polyhedra and is overall neutral. If the charge distribution in the ISR is decomposable into symmetric neutral cells as assumed in the NPT, the ISR would have no effect on the BO and may be removed entirely, leaving behind only the two NPT model solids separated by vacuum. The VBO for such a gapped charge distribution is simply the difference in VBM positions of the two oxide model solids that can be found in Table II. However, to model the potential distribution at the interface more carefully, the

TABLE I. Properties of bulk perovskite oxide as analyzed by Bader's atoms-in-molecules method. The charges of Bader atoms are listed. The VBM positions of model solids constructed with Bader atoms listed are calculated with the HSE functional. Corner-cation-centered (CCC) unit cells and body-center-atom-centered (BAC) unit cells are used to construct two model solids for each bulk oxide. VBM positions of model solids constructed to model (110), mixed-BC (111), and mixed-CNR (111) interfaces are also listed. These values are obtained by taking adjustments due to shifts in atomic positions from the CCC or the BAC model solids, as explained in detail in the Supplemental Material [40].

Oxide	CNR Bader charge (e)	BC Bader charge (e)	Oxygen Bader charge (e)	VBM CCC (Mx-BC (100)) (eV)	VBM BAC (Mx-CNR (100)) (eV)	VBM (110) (eV)	VBM Mx-BC (111) (eV)	VBM Mx-CNR (111) (eV)
SrTiO ₃	1.58	2.14	-1.24	-4.58	-0.66	-9.74	1.48	-6.71
LaGaO ₃	2.08	1.69	-1.26	-6.93	2.56	-9.40	1.05	-5.42
NdGaO ₃	2.12	1.69	-1.27	-7.11	2.67	-9.51	1.01	-5.45
PbTiO ₃	1.38	2.16	-1.18	-3.56	-1.26	-9.15	1.70	-6.52
NaTaO ₃	0.89	2.54	-1.15	-2.19	-5.08	-10.16	1.20	-8.47
BaTiO ₃	1.51	2.14	-1.22	-4.35	-1.06	-9.56	1.32	-6.73
NaNbO ₃	0.90	2.57	-1.16	-2.33	-5.24	-10.28	1.03	-8.60
KTaO ₃	0.80	2.53	-1.11	-1.77	-5.23	-9.76	1.25	-8.25
CaSnO ₃	1.62	2.49	-1.37	-4.35	-1.58	-10.58	1.65	-7.58
KNbO ₃	0.81	2.55	-1.12	-1.95	-5.38	-9.90	1.06	-8.39
SrSnO ₃	1.61	2.46	-1.36	-4.31	-1.51	-10.37	1.59	-7.41
CaHfO ₃	1.62	2.45	-1.36	-4.26	-1.34	-10.25	1.69	-7.28
CaZrO ₃	1.63	2.47	-1.37	-4.25	-1.42	-10.30	1.66	-7.34
SrHfO ₃	1.61	2.45	-1.35	-4.07	-1.28	-10.05	1.78	-7.12
BaSnO ₃	1.56	2.41	-1.32	-4.22	-1.66	-10.11	1.41	-7.29
SrZrO ₃	1.61	2.47	-1.36	-4.08	-1.37	-10.08	1.73	-7.17
PbZrO ₃	1.35	2.50	-1.28	-3.34	-2.59	-9.92	1.54	-7.48
NdInO ₃	2.12	1.59	-1.24	-6.94	2.60	-8.87	0.70	-5.05
BaZrO ₃	1.54	2.47	-1.34	-3.77	-1.56	-9.83	1.75	-7.08
LaInO ₃	2.11	1.60	-1.24	-6.89	2.48	-8.84	0.66	-5.07

TABLE II. Charge distribution in bulk perovskite oxide analyzed by the method of neural polyhedra theory. The potential energy, face density, and VBM are the average potential energy, the charge density at the surface, and the valence-band maximum position calculated with the HSE functional, respectively, of model-solids constructed from neutral polyhedra of bulk oxides. The average charge density in the volume bound by neutral polyhedra and Bader atoms is listed as intermediate density.

Oxide	Lattice constant (Å)	NPT mod. sol.		Intermediate density ($e/\text{Å}^3$)	NPT mod. sol. VBM (eV)
		Avg. pot. eng. (eV)	Face density ($e/\text{Å}^3$)		
SrTiO ₃	3.940	-12.74	0.22	0.18	-4.29
LaGaO ₃	3.940	-13.12	0.20	0.19	-4.29
NdGaO ₃	3.940	-12.50	0.20	0.17	-4.31
PbTiO ₃	3.970	-9.20	0.22	0.15	-4.94
NaTaO ₃	3.970	-13.93	0.21	0.20	-4.02
BaTiO ₃	4.020	-13.56	0.21	0.18	-4.51
NaNbO ₃	4.020	-9.99	0.21	0.18	-4.92
KTaO ₃	4.020	-10.24	0.21	0.14	-5.06
CaSnO ₃	4.070	-12.16	0.24	0.16	-4.75
KNbO ₃	4.070	-10.97	0.20	0.17	-5.06
SrSnO ₃	4.115	-12.68	0.23	0.16	-4.83
CaHfO ₃	4.115	-12.02	0.23	0.15	-4.83
CaZrO ₃	4.145	-11.81	0.22	0.14	-4.67
SrHfO ₃	4.145	-12.42	0.23	0.16	-4.65
BaSnO ₃	4.180	-13.48	0.23	0.17	-4.96
SrZrO ₃	4.180	-12.36	0.23	0.15	-4.69
PbZrO ₃	4.180	-13.52	0.22	0.17	-4.84
NdInO ₃	4.180	-11.34	0.20	0.14	-4.33
BaZrO ₃	4.220	-13.29	0.22	0.17	-4.74
LaInO ₃	4.220	-11.67	0.22	0.14	-4.39

disparity in the average charge densities on the surfaces of the two NPT model solids, as listed in Table II, needs to be handled. As shown previously for zinc-blende heterojunctions [34,35] and explained in detail in Discussion SM3 in the SM [40], the expected smoothing of densities on the surfaces when different model solids are stitched necessitates a correction to the NPT. The horizontal solid bars in Figs. 2 and 4 are NPT predictions with the polyhedra face density difference (found in Table II) assumed to linearly “smear out” over a distance of $\frac{1}{4}a$ (where a is the cubic lattice constant).

The good agreement of NPT predictions with the DFT-computed, relaxed, VBOs seems to suggest that the charge distribution at perovskite oxide interface indeed can be approximately partitioned into symmetric neutral cells. The length chosen for charge smoothing in perovskite oxides here is similar, in relationship to the shortest interatomic distance, to that previously used for zinc-blende heterojunctions [34]. As the perovskite oxides presently studied span groups of different valences, the actual chemistry at their interfaces may be varied. For heterovalent systems, the sizes of the neutral polyhedra (or the sizes of the Bader atoms, see Table SM3 of the SM [40]) are typically poorly matched across the interface. The expected volumetric adjustments at some heterojunctions may lead to charge relaxation effects beyond what can be accounted for by face density correction. For significant charge rearrangement, a more representative charge density for the bulk oxides is that in the entire region/volume away from the ion cores. The availability of NPT and Bader analysis data actually provides an easy and reasonable estimate of the average density in the “intermediate region” of the unit cell: The number of excess electrons in the oxygen Bader atom divided by the volumetric difference between the oxygen neu-

tral polyhedron and the oxygen Bader atom well represents, and is here called, the “intermediate density” for a perovskite oxide. For example, dividing the number of the excess electrons in an oxygen Bader atom in SrTiO₃, 1.24 (Table I), by the oxygen volume difference, $12.50 - 5.50 = 7.00 \text{ Å}^3$ (Table SM3 of the SM [40]), gives $0.177 e/\text{Å}^3$, which is the value listed in Table II as the intermediate density for SrTiO₃. The assumption that the intermediate density difference smooths out over a length of $1/3a$ provides an alternative correction to the NPT, listed under “NPT (interm. dens.)” in Table III and shown as horizontal broken lines on Fig. 4(a) for heterovalent interfaces. The difference between solid and broken horizontal bars in Fig. 4(a) may be viewed as an inherent uncertainty in NPT analysis, as it reflects how NPT could be affected by typical assumptions on the charge smoothing.

V. DISCUSSION

The bulklike behavior of BO is well known for various heterojunction interfaces and it has dominated theoretical models for heterojunction BO [1]. It has been inferred from the bulklike BO that the band edges of semiconductors can be placed on a universal scale, with the difference between two semiconductors on that scale being the magnitude of the BO at their heterojunction [1]. Analysis based on Eq. (1), however, makes it clear that the magnitude of BO is, in general, intimately related to equilibrium charge distribution at the interface. The observed tunability and nontransitivity of BO at heterovalent interfaces also attests to the important role played by the interface in BO formation [11,12,35]. The bulklike behavior of BO observed for some heterojunctions thus necessarily reflects a particular property of those relaxed

TABLE III. Valence-band offset (eV) calculated for relaxed heterojunctions between perovskite oxides. The VBO is the VBM position of the first oxide subtract the VBM of the second oxide, both calculated with the HSE functional. For heterovalent heterojunctions with polar (100) and (111) orientations, the interface calculated has either mixed corner-cation atoms (Mx-CR) or mixed body-center metal atoms (Mx-BC) on the interface plane. For isovalent heterojunctions with polar orientations, the stacking sequence is either corner atom of first oxide to body-center atom of second oxide (CR1-BC2) or body-center atom of first oxide to corner atom of second oxide (BC1-CR2) at the interface. Listed under “NPT (f. dens.)” and “NPT (interm. dens.)” are VBO’s modeled with NPT, using corrections based on polyhedra-face and intermediate densities, respectively.

Hetero-junction	Mx-Cnr or Cr1-BC2 (100)	Mx-BC or Cr2-BC1 (100)	Planar (110)	Mx-Cnr or Cr1-BC2 (111)	Mx-BC or Cr2-BC1 (111)	NPT (f. dens.)	NPT (interm. dens.)
SrTiO ₃ /LaGaO ₃	-0.114	0.007	0.012	-0.091	-0.084	-0.112	
SrTiO ₃ /NdGaO ₃	-0.163	-0.033	-0.023	-0.079	-0.129	-0.101	
LaGaO ₃ /NdGaO ₃	-0.035		-0.129	-0.041		0.011	
PbTiO ₃ /NaTaO ₃	0.891	0.760	0.829	0.708	0.820	0.989	
BaTiO ₃ /KTaO ₃	0.300	0.279	0.199	0.199	0.249	0.427	0.324
BaTiO ₃ /NaNbO ₃	0.126	0.213	0.237	0.061	0.106	0.520	-0.023
KTaO ₃ /NaNbO ₃	0.027	0.086	-0.051	-0.041	-0.022	0.093	-0.347
CaSnO ₃ /KNbO ₃	0.265	0.162	0.195	0.103	0.152	0.028	0.456
CaHfO ₃ /SrSnO ₃	0.296	0.264	0.311	0.164	0.099	-0.012	0.206
CaZrO ₃ /SrHfO ₃	0.124	0.083	0.104	0.090	0.094	0.010	0.175
BaSnO ₃ /SrZrO ₃	-0.174	-0.329	-0.327	-0.191	-0.331	-0.265	
BaSnO ₃ /PbZrO ₃	-0.089	-0.128	-0.166	-0.092	-0.249	-0.202	
SrZrO ₃ /PbZrO ₃	-0.004		0.040	0.096		0.064	
SrZrO ₃ /NdInO ₃	-0.651	-0.913	-0.691	-0.673	-0.822	-0.568	
BaZrO ₃ /LaInO ₃	-0.893	-0.904	-0.677	-0.798	-0.892	-0.359	-0.743

interfaces, namely, the shift in the average potential energy across such an interface is insensitive to its atomic structure and orientation. The present perovskite oxide heterojunctions, as well as previously investigated isovalent zinc-blende heterojunctions, all display bulklike BOs that agree with the predictions of NPT [34]. This agreement thus identifies another important property of the bulklike BO: the shift in potential energy across the ISR of such an interface, or the total dipole moment of the ISR, vanishes. As pointed out above, this property is well expected when the charge distribution in the ISR is stackable from symmetric neutral cells, a key assumption in NPT. Because the charge distribution is the result of energy minimization, one comes to the deduction that a charge distribution that minimizes the energy in the ISR does not contribute to an overall potential energy shift. This suggests a possible connection between energy minimization and a charge density approximately constructible from symmetric neutral cells. For ionic compounds, the total energy is dominated by the electrostatic potential energy, the minimization of which amounts to a reduction in the average electric field strength or the energy stored in the electric field. For covalent compounds and interfaces, a minimization in energy associated with electric field is also an important factor governing the formation of charge distribution. NPT partitions the equilibrium charge density into neutral polyhedra with internal charge distributions that satisfy the chemical driving force of the system and, at the same time, confine the electric field due to its own charge to within each polyhedron. The lack of net electrostatic interactions between neutral polyhedra naturally minimizes the electric field and energy. It is this connection between neutral polyhedra and energy minimization that is likely behind the success of the NPT in predicting the BOs for both ionic-type and covalent-type heterojunctions. Being well in line with the concept of nearsightedness in quantum

mechanical systems [36], this connection is an essential part of the explanation of the bulklike behavior of BO. In the absence of heterovalent covalent bonds, the charge density distribution at the interface is likely symmetric about atomic sites to minimize the electrostatic potential energy, leading to BOs that are bulklike.

A dependence of the BO on the atomic arrangement and orientation of the interface, when observed, suggests asymmetry in charge distribution around some atoms at the interface. Symmetry in local charge distribution about atomic positions cannot be maintained at these interfaces and the NPT alone cannot account for the BO, likely because of the dominance of bond chemistry in the total energies of such systems. Among systems considered thus far, significant BO tunability was only found for heterojunctions between heterovalent zinc-blende semiconductors. These covalently bonded systems are known to incur significant charge transfer among interface atoms involved in heterovalent bonds [35]. Such charge transfers and the accompanying local asymmetry in charge distribution about atomic positions contribute to net dipole moments from the ISR of these interfaces. For heterovalent zinc-blende interfaces, such dipolar contributions were successfully modeled, using the concept of dielectric screening, as corrections to the BO predicted by NPT [35]. The well-known large ionic contribution to the static dielectric constants of perovskite oxides [58], as illustrated in Figs. 5 and 6, is apparently responsible for both the lack of significant charge transfer and the bulklike behavior displayed by BO at their heterojunctions. Therefore, the entire behavior of the BO presently found for perovskite oxide heterojunctions is nearly identical to that previously reported for zinc-blende heterojunctions [34,35], when the large static dielectric constants of the oxides are considered, but here they are dominated by the ionic, rather than the electronic, response.

Although the absence of electric field on all atomic sites is obviously a condition that is satisfied in all previous studies of relaxed solid interfaces, it has not been recognized as crucial for the explanation of the bulklike BO behavior. The vanishing of electric field is generally conducive to symmetry in the local charge density about each atomic site, which in turn underpins the simplicity offered by partitioning the interface charge density into neutral symmetric cells. While the equilibrium charge distribution of the entire relaxed interface, which is daunting to predict, controls the magnitude of the BO, the validity of such a partition obviates the need for detailed knowledge of the interface charge distribution in accurately predicting the BO. When NPT was proposed to account for the BOs of the covalent zinc-blende heterojunctions, the expectation was (with evidence given) that a model charge distribution stitched together with those of NPT model solids would resemble the equilibrium charge distribution at the relaxed interface [34]. With lessons learned from the present work on perovskite oxide interfaces, it now appears that the validity of the NPT depends only on the symmetry in local charge distribution about atoms at the interface, and not necessarily the ability to accurately predict the charge distribution as such. The task of predicting and understanding heterojunction BOs is thus simplified drastically.

VI. CONCLUSIONS

In the present work, the formation of BOs at a large number of lattice-matched interfaces between perovskite oxides is studied numerically using DFT. Ionic screening is found to render the BO of a relaxed heterojunction essentially independent of the atomic structure and the orientation of the interface, i.e., to be bulklike. Through analysis of the requirement of zero electric fields on all atomic sites of a relaxed interface, NPT is justified and shown to well account for calculated BOs at perovskite oxide heterojunctions. The success of the NPT, presently for ionic interfaces and previously for covalent zinc-blende interfaces, unmarks a connection between energy minimization and the partition of interface charge distribution into neutral symmetric cells. The bulklike behavior of BO, experimentally observed and numerically calculated for various heterojunctions, stems directly from such a connection. As energy minimization governs the formation of charge distribution in general, NPT is expected to describe the band offsets at a wide variety of material interfaces.

ACKNOWLEDGMENT

We thank Dr. Ariel Biller for assistance with the calculations.

-
- [1] A. Franciosi and C. G. Van de Walle, *Surf. Sci. Rep.* **25**, 1 (1996).
 - [2] V. V. Afanas'ev, H. Y. Chou, M. Houssa *et al.*, *Appl. Phys. Lett.* **99**, 172101 (2011).
 - [3] T. M. Duc, C. Hsu, and J. P. Faurie, *Phys. Rev. Lett.* **58**, 1127 (1987).
 - [4] S. Li, F. Chen, R. Schafrank *et al.*, *Phys. Stat. Sol. Rapid Res. Lett.* **8**, 571 (2014).
 - [5] E. T. Yu, J. O. McCaldin, and T. C. McGill, *Solid State Phys.* **46**, 1 (1992).
 - [6] J. Tersoff, *Phys. Rev. B* **30**, 4874 (1984).
 - [7] M. Cardona and N. E. Christensen, *Phys. Rev. B* **35**, 6182 (1987).
 - [8] P. W. Peacock and J. Robertson, *Phys. Rev. Lett.* **92**, 057601 (2004).
 - [9] J. Tersoff and W. A. Harrison, *Phys. Rev. Lett.* **58**, 2367 (1987).
 - [10] C. G. Van de Walle and J. Neugebauer, *Nature (London)* **423**, 626 (2003).
 - [11] J. R. Waldrop and R. W. Grant, *Phys. Rev. Lett.* **43**, 1686 (1979).
 - [12] X. Wang, J. Xiang, W. Wang *et al.*, *Appl. Phys. Lett.* **102**, 031605 (2013).
 - [13] C. Maierhofer, S. Kulkarni, M. Alonso, T. Reich, and K. Horn, *J. Vac. Sci. Technol. B* **9**, 2238 (1991).
 - [14] E. T. Yu, M. C. Phillips, D. H. Chow, D. A. Collins, M. W. Wang, J. O. McCaldin, and T. C. McGill, *Phys. Rev. B* **46**, 13379 (1992).
 - [15] A. Pramanick, A. D. Prewitt, J. S. Forrester, and J. L. Jones, *Crit. Rev. Solid State Mater. Sci.* **37**, 243 (2012).
 - [16] G. Liu, S. Zhang, W. Jiang, and W. Cao, *Mater. Sci. Eng. Rep.* **89**, 1 (2015).
 - [17] J. Wu, Z. Fan, D. Xiao, J. Zhu, and J. Wang, *Prog. Mater. Sci.* **84**, 335 (2016).
 - [18] D. S. Jeong, R. Thomas, R. S. Katiyar, J. F. Scott, H. Kohlstedt, A. Petraru, and C. S. Hwang, *Rep. Prog. Phys.* **75**, 076502 (2012).
 - [19] A. Ohtomo and H. Y. Hwang, *Nature (London)* **427**, 423 (2004).
 - [20] H. Y. Hwang, Y. Iwasa, M. Kawasaki, B. Keimer, N. Nagaosa, and Y. Tokura, *Nat. Mater.* **11**, 103 (2012).
 - [21] L. Bjaalie, B. Himmetoglu, L. Weston, A. Janotti, and C. G. Van de Walle, *New J. Phys.* **16**, 025005 (2014).
 - [22] P. Moetakef, T. A. Cain, D. G. Ouellette *et al.*, *Appl. Phys. Lett.* **99**, 232116 (2011).
 - [23] J. Robertson, *EPJ Appl. Phys.* **28**, 265 (2004).
 - [24] S. A. Chambers, L. Qiao, T. C. Droubay, T. C. Kaspar, B. W. Arey, and P. V. Sushko, *Phys. Rev. Lett.* **107**, 206802 (2011).
 - [25] R. Comes and S. Chambers, *Phys. Rev. Lett.* **117**, 226802 (2016).
 - [26] A. Giampietri, G. Drera, and L. Sangaletti, *Adv. Mater. Interf.* **4**, 1700144 (2017).
 - [27] A. Alkauskas, P. Broqvist, F. Devynck, and A. Pasquarello, *Phys. Rev. Lett.* **101**, 106802 (2008).
 - [28] K. Steiner, W. Chen, and A. Pasquarello, *Phys. Rev. B* **89**, 205309 (2014).
 - [29] A. Krishnapriyan, P. T. Barton, M. Miao, and R. Seshadri, *J. Phys.: Condens. Matter* **26**, 155802 (2014).
 - [30] D. Colleoni, G. Miceli, and A. Pasquarello, *Appl. Phys. Lett.* **107**, 211601 (2015).
 - [31] Y. Hinuma, Y. Kumagai, I. Tanaka, and F. Oba, *Phys. Rev. B* **95**, 075302 (2017).
 - [32] R. T. Tung, *Mater. Sci. Eng. Rep.* **35**, 1 (2001).

- [33] R. T. Tung, *Appl. Phys. Rev.* **1**, 011304 (2014).
- [34] R. T. Tung and L. Kronik, *Phys. Rev. B* **94**, 075310 (2016).
- [35] R. T. Tung and L. Kronik, *Adv. Theory Simul.* **1**, 1700001 (2018).
- [36] W. Kohn, *Phys. Rev. Lett.* **76**, 3168 (1996).
- [37] N. Nakagawa, H. Y. Hwang, and D. A. Muller, *Nat. Mater.* **5**, 204 (2006).
- [38] L. Qiao, T. C. Droubay, V. Shutthanandan, Z. Zhu, P. V. Sushko, and S. A. Chambers, *J. Phys.: Condens. Matter* **22**, 312201 (2010).
- [39] A. Janotti, L. Bjaalie, L. Gordon, and C. G. Van De Walle, *Phys. Rev. B* **86**, 241108 (2012).
- [40] See Supplemental Material at <http://link.aps.org/supplemental/10.1103/PhysRevB.99.115302> for discussions on Bader model solids, correction due to charge density difference, minimized spherapole sum from NPT, and other scientific issues.
- [41] G. Kresse and J. Hafner, *Phys. Rev. B* **49**, 14251 (1994).
- [42] G. Kresse and J. Furthmuller, *Phys. Rev. B* **54**, 11169 (1996).
- [43] G. Kresse and D. Joubert, *Phys. Rev. B* **59**, 1758 (1999).
- [44] J. P. Perdew, K. Burke, and M. Ernzerhof, *Phys. Rev. Lett.* **77**, 3865 (1996).
- [45] J. P. Perdew, M. Ernzerhof, and K. Burke, *J. Chem. Phys.* **105**, 9982 (1996).
- [46] J. Heyd, G. E. Scuseria, and M. Ernzerhof, *J. Chem. Phys.* **118**, 8207 (2003).
- [47] A. V. Krukau, O. A. Vydrov, A. F. Izmaylov, and G. E. Scuseria, *J. Chem. Phys.* **125**, 224106 (2006).
- [48] P. Broqvist, J. F. Binder, and A. Pasquarello, *Microelectron. Eng.* **88**, 1467 (2011).
- [49] S. Hong, S. M. Nakhmanson, and D. D. Fong, *Rep. Prog. Phys.* **79**, 076501 (2016).
- [50] R. F. W. Bader, *Acc. Chem. Res.* **18**, 9 (1985).
- [51] R. F. W. Bader, A. Larouche, C. Gatti, M. T. Carroll, P. J. MacDougall, and K. B. Wiberg, *J. Chem. Phys.* **87**, 1142 (1987).
- [52] G. Henkelman, A. Arnaldsson, and H. Jonsson, *Computa. Mater. Sci.* **36**, 354 (2006).
- [53] W. Tang, E. Sanville, and G. Henkelman, *J. Phys.: Condens. Matter* **21**, 084204 (2009).
- [54] C. G. Van de Walle and R. M. Martin, *Phys. Rev. B* **35**, 8154 (1987).
- [55] S. A. Chambers, T. C. Kaspar, A. Prakash, G. Haugstad, and B. Jalan, *Appl. Phys. Lett.* **108**, 152104 (2016).
- [56] R. P. Feynman, *Phys. Rev.* **56**, 340 (1939).
- [57] R. T. Tung and L. Kronik (unpublished).
- [58] *Handbook of Optical Constants of Solids*, edited by E. D. Palik (Academic Press, Cambridge, MA, 1997).